

# Surface Phase Diagrams for Wetting on Heterogenous Substrates

C. Rascón\* and A. O. Parry

*Department of Mathematics, Imperial College  
180 Queen's Gate, London SW7 2BZ, United Kingdom*

We propose a simplified description of fluid adsorption on heterogenous micropatterned substrates. Using this approach, we are able to rederive results obtained earlier using effective interfacial Hamiltonian methods and predict a number of new examples of surface phase behaviour for both singly and periodically striped substrates. In particular, we show that, for a singly striped system, the manner in which the locus of surface unbending phase transitions approaches the pre-wetting line of the infinite pure system, in the limit of large stripe widths, is non-trivial and sensitive to several characteristic lengthscales and competing free-energies. For periodic substrates, we investigate finite-size deviations from Cassie's law for the wetting temperature of the heterogeneous system when the domain sizes are mesoscopic.

PACS numbers: 68.08.B, 68.43, 68.35.R, 68.35.M

## I. INTRODUCTION

Fluid interfacial phenomena on flat, homogeneous substrates have drawn enormous attention over the last few decades [1]. However, present experimental methods allow an ever increasing control over the shape and chemical composition of solid surfaces and pose more demanding challenges for both theory and experiments. These advances make the study of adsorption on non-planar and heterogeneous substrates inevitable. Recent experimental and theoretical studies have shown that structured substrates exhibit a variety of novel adsorption properties which not only promise to be of importance to future technologies such as microfluidics [2], but are also of fundamental interest to statistical physics [3]. In particular, the effect of chemical inhomogeneities has been addressed recently in different contexts, for example: contact angles of liquid drops [4–6], droplet spreading [7], morphological phase transitions [8], three phase contact line [9], Cassie's law [10,11], drop shapes [12], construction of magnetic materials [13], microscopic packing [14], liquid channels [15], polymer blends [16,17], and dewetting [18], among others.

In this paper, we concentrate on the equilibrium wetting properties of flat but chemically structured substrates. Specifically, we study liquid adsorption in two representative micropatterned systems: a homogeneous substrate with a single distinct chemical stripe and a substrate comprising parallel stripes of two different materials. These systems have been partially studied by other authors with the help of density functional theory [14,19] and effective interfacial methods [20–22]. Nonetheless,

the intrinsic complexity of those formulations does not allow a thorough exploration of the vast space of possible surface phase behaviour these systems offer. We propose here a minimal model to understand the general wetting properties of these systems. The model, described in section II, appears to capture the essential physics of the problem in a qualitative manner and recovers former results obtained with more sophisticated methods for particular cases. The great advantage of the minimal model is that it allows us to obtain (sections of) global surface phase diagrams and explore what kind of surface phase behaviour is possible in such heterogeneous systems. As we shall show, in spite of the simplicity of the model, the ensuing surface phase behaviour is extremely rich. In section III, the model is applied to a substrate with a single stripe of a different material, while in section IV, a periodic substrate made of parallel stripes of two materials is studied. We finish our article with a summary of our main conclusion and a discussion of further work.

## II. MINIMAL MODEL

Consider two flat substrates made of different materials (labelled 1 and 2) whose adsorption properties can be described, when homogeneous, by effective potentials  $W_1(\ell)$  and  $W_2(\ell)$ , respectively [23]. When each of these substrates is exposed to a near saturated gas, a liquid layer is adsorbed on its surface, whose thickness  $\ell_1^\pi$  (or  $\ell_2^\pi$ ) is given by the position of the absolute minimum of the corresponding effective potential (the superscript  $\pi$  denotes behaviour characteristic of the pure homogeneous substrate). We suppose the wetting temperatures of each of these systems are  $T_w^{(1)}$  and  $T_w^{(2)}$ , respectively. Consider now a flat substrate  $\Lambda$  consisting of domains  $\Lambda_1$  and  $\Lambda_2$  (not necessarily connected) made of materials 1 and 2, respectively. When this microprinted substrate is exposed to a gas, a liquid layer is adsorbed on its surface, whose equilibrium thickness profile  $\ell(x, y)$  must show considerable spatial dependence (especially strong close to the boundaries between the domains). For mesoscopic domains, this dependence can be captured by an effective interfacial description: the equilibrium profile of the adsorbed liquid layer will minimise the following free-energy functional

$$\mathcal{H}[\ell] = \int_{\Lambda} d\mathbf{r} \frac{\Sigma}{2} (\nabla\ell)^2 + \int_{\Lambda_1} d\mathbf{r} W_1(\ell) + \int_{\Lambda_2} d\mathbf{r} W_2(\ell), \quad (1)$$

where  $\Sigma$  is the liquid-vapour interfacial tension. This model assumes a sharp crossover in the local form of the

effective potential at the domains boundaries and is itself an approximation to a more realistic description in which this crossover is smooth [20]. However, this assumption certainly does not alter the global structure of the surface phase behaviour [9]. To continue, and for the sake of simplicity, we only consider systems translationally invariant along the  $y$  axis (see Fig. 1). Therefore, the equilibrium profile will follow from the minimisation of the somewhat simpler functional

$$H[\ell] = \int_{\mathcal{L}} dx \frac{\Sigma}{2} \dot{\ell}^2 + \int_{\mathcal{L}_1} dx W_1(\ell) + \int_{\mathcal{L}_2} dx W_2(\ell), \quad (2)$$

where the dot represents differentiation with respect to  $x$ , and  $\mathcal{L}$ ,  $\mathcal{L}_1$  and  $\mathcal{L}_2$  are the appropriate linear domains corresponding to sections of  $\Lambda$ ,  $\Lambda_1$  and  $\Lambda_2$ , respectively. This approach has been employed by a number of authors to obtain numerical solutions of the equilibrium profile for a substrate with a single stripe of a different material (Fig. 1(a)) [20–22]. Their results show that if the width of the stripe  $L_1$  is very large, the thickness of the adsorbed layer is essentially the same as in the pure systems within each of the domains ( $\ell_1^\pi$  in  $\Lambda_1$ ,  $\ell_2^\pi$  in  $\Lambda_2$ ), and varies abruptly in the domain borders. In other words, for large stripe widths, the minimisation of (2) is achieved by a local minimisation of the second and third terms of the functional. The (positive) contribution of the first term in (2), which originates in the domain borders, is practically negligible. We can estimate this latter contribution by noticing that the characteristic length for lateral variations of the interface profile is given roughly by the transverse correlation lengths  $\xi_{\parallel}^{(i)} = \sqrt{\Sigma/W''(\ell_i^\pi)}$  of the homogeneous substrates  $i=1, 2$ . Thus, for a single step, we can write

$$\int dx \frac{\Sigma}{2} \dot{\ell}^2 \approx \frac{\kappa}{2} (\ell_1^\pi - \ell_2^\pi)^2 \quad (3)$$

with  $\kappa \equiv \Sigma/(\xi_{\parallel}^{(1)} + \xi_{\parallel}^{(2)})$ . For smaller values of  $L_1$ , however, this energetic contribution becomes comparable to that arising from the second term of (2) and the interface adopts distinct configurations in order to minimise the free-energy of the system. This gives rise to certain surface phase transitions, denoted surface condensation or *unbending* transitions, in which different liquid interfacial configurations coexist [20–22,24]. In order to calculate the loci of these transitions in the  $T$ - $\mu$  diagram, the free-energy functional (2) must be minimised for different values of the temperature  $T$  and the chemical potential  $\mu$ . Although this has been done for a specific case [21], the vast space of parameters involved and the arduous task of minimising the functional (2) does not allow a thorough exploration of the physics of the system and impedes a systematic study of more complex systems, for instance, a periodic array of stripes (see Fig. 1(b)).

Here we propose a minimal model to describe the overall phenomenology of the above mentioned surface *unbending* transitions in a simple and illuminating manner.

To do that, we approximate the free-energy *functional* (2) by a free-energy *function* of a finite number of variables. By doing that, we lose the detailed description of the shape of the adsorbed layer (which follows from the minimisation of Eq. (2)), but, as explained here, we capture the fundamental physical mechanism for the surface phase transitions underlying (2). To start, we define a collective coordinate  $\ell_i$  for every connected region of each of the domains. This coordinates will account for the *average* thickness (in a loose manner) of the adsorbed layer within that connected region and it is defined implicitly as follows

$$L_i W_\alpha(\ell_i) = \int_{L_i} dx W_\alpha(\ell), \quad (4)$$

$L_i$  being the width of the connected region and  $\alpha = 1$  or 2, depending on the domain that region belongs to. Within the minimal model, we consider these collective coordinates as independent entities, to be varied in order to minimise the free-energy. This accounts for the second and third integrals of (2) which are replaced by a sum over terms  $L_i W_\alpha(\ell_i)$ , one for each connected region. To obtain a full description in terms of these variables, we simply estimate the contribution of the first term of (2) similar to that shown in Eq. (3) but using the collective coordinates. Thus, the free-energy functional is reduced to a function of a small number of real variables. Specifically, for the periodic array of stripes (Fig. 1(b)), we write the free-energy per period as

$$H(\ell_1, \ell_2) = \kappa (\ell_1 - \ell_2)^2 + L_1 W_1(\ell_1) + L_2 W_2(\ell_2). \quad (5)$$

In accordance with our aim of developing a minimal description, we consider  $\kappa$  constant throughout the paper (independent of the temperature and the chemical potential).

The free-energy for a substrate with a single stripe (Fig. 1(a)) can be obtained from (5) in the limit  $L_2 \rightarrow \infty$ . In this case, the last term of (5) becomes the most important and it must be minimised fully, yielding  $\ell_2 = \ell_2^\pi$ . Subtracting this (infinite) constant contribution from the free-energy, the average thickness of the adsorbed layer on the stripe will follow from the minimisation of

$$H(\ell_1) = \kappa (\ell_1 - \ell_2^\pi)^2 + L_1 W_1(\ell_1). \quad (6)$$

The generalization of this procedure to more sophisticated geometries is straightforward. As an example, the average thickness  $\ell_1$  of the adsorbed layer on a circle of radius  $R$  made of material 1 on a substrate made of material 2 could be obtained from the minimization of

$$H(\ell_1) = \pi R \kappa (\ell_1 - \ell_2^\pi)^2 + \pi R^2 W_1(\ell_1), \quad (7)$$

where an appropriate  $\kappa$  now accounts for the energy due to the curvature of the interface. It is likely that this procedure will fail to work for certain intricate shape domains where more complicated behaviour may be expected.

We stress here that this approach does not intend to be a quantitative description of these phenomena but to capture the essential features of heterogeneous adsorption, which, due to the complexity of the available models, remain mainly unexplored.

### III. SINGLE STRIPE

#### A. General Considerations

Here we apply the model described above to a homogeneous flat substrate with an infinite length stripe of width  $L_1$  (Fig. 1(a)). Before presenting the results, however, we make a number of pertinent remarks concerning general aspects of the surface phase behaviour:

- For small values of the stripe width, corresponding to the limit  $L_1 \rightarrow 0$ , we expect that the thickness of the layer adsorbed on the stripe will tend to the thickness of the liquid layer absorbed on the outer substrate, *i.e.*  $\ell_1 \rightarrow \ell_2^\pi$ .
- If the stripe width is large, corresponding to the limit  $L_1 \rightarrow \infty$ , the thickness of the layer adsorbed on the stripe will tend to the thickness of the liquid layer absorbed on a homogeneous flat substrate of material 1, *i.e.*  $\ell_1 \rightarrow \ell_1^\pi$ .
- If the thickness of the adsorbed layers on both infinite substrates is the same ( $\ell_1^\pi = \ell_2^\pi$ ), the functional (2) is fully minimised by a flat solution  $\ell(x) = \ell_1^\pi = \ell_2^\pi$ . The loci of the points for which  $\ell_1^\pi = \ell_2^\pi$  constitute a line in the  $T - \mu$  phase diagram and separates interfacial profiles with different convexity [25]. Observe that the flat solution corresponds to the minimisation of *each* term of the functional and cannot be improved by any other configuration. It follows that such a solution will be the global equilibrium for arbitrary values of the stripe width  $L_1$ . In turn, this implies that no first-order surface coexistence line can cross the line defined implicitly by  $\ell_1^\pi = \ell_2^\pi$ . As explained below, this simple observation severely constrains the possible topology of the surface phase diagram. Intriguingly, the loci of points satisfying  $\ell_1^\pi = \ell_2^\pi$  represents surface phases which are fully homogeneous on the heterogeneous substrate.
- Any first-order phase boundary corresponding to a line of coexistence in the  $T - \mu$  plane satisfies a Clausius-Clapeyron-like equation [26]:

$$\left(\frac{d\mu}{dT}\right)_{\text{coex}} = -\frac{\Delta S}{\Delta \Gamma}, \quad (8)$$

where  $\Delta S$  and  $\Delta \Gamma$  are the differences in surface entropy and adsorption between the coexisting phases,

respectively, which follow in the usual manner from the free-energy of the system  $\omega(T, \mu) = \min H$  as  $S \equiv -(\partial\omega/\partial T)_\mu$  and  $\Gamma \equiv -(\partial\omega/\partial\mu)_T$ .

For our purposes, it is more convenient to measure the slope of this line with respect to that of the liquid-vapour coexistence curve  $\mu_{LV}(T)$ . Thus, we rewrite Eq. (8) as

$$\left(\frac{d\Delta\mu}{d\Delta T}\right)_{\text{coex}} = -\frac{\Delta\tilde{S}}{\Delta\tilde{\Gamma}}, \quad (9)$$

where  $\Delta\mu \equiv (\mu_{LV} - \mu)$ ,  $\Delta T \equiv T - T_w$  (for a given wetting temperature),  $\tilde{S} \equiv -(\partial\omega/\partial\Delta T)_{\Delta\mu}$  and  $\tilde{\Gamma} \equiv -(\partial\omega/\partial\Delta\mu)_{\Delta T} = -\Gamma$ .

#### B. Minimal Model

The equilibrium value of the *average* thickness  $\ell_1(T, \mu, L_1)$  follows from the minimisation of the minimal free-energy (6), yielding

$$2\kappa(\ell_1 - \ell_2^\pi) + L_1 W_1'(\ell_1) = 0. \quad (10)$$

This equation has a straightforward graphical interpretation from which one can elegantly glean the possible surface phase behaviour. To see this, we rewrite the equation as

$$W_1'(\ell_1) = \frac{2\kappa}{L_1}(\ell_2^\pi - \ell_1), \quad (11)$$

corresponding to the intersection of a straight line with a curve. The general form of the graphical construction is illustrated in Fig. 2 for a specific choice of effective potential. Note the following features:

- The model always shows at least one solution. Multiple solutions correspond to the presence of first-order surface phase transitions.
- The straight line has a negative slope inversely proportional to the stripe width and necessarily crosses the horizontal axis at  $\ell_2^\pi$ .
- The curve always intersects the horizontal axis at  $\ell_1^\pi$  (but may exhibit other crossings) and tends to  $\Delta\mu \delta\rho$  as  $\ell_1 \rightarrow \infty$ . Here,  $\delta\rho$  represents the difference in bulk densities of the coexisting liquid and gas states.
- For any given temperature and chemical potential, only three scenarios are possible within the graphical construction. These correspond to the straight line intersecting the curve at one, two or three points. In the first scenario [Fig. 2(a) or (b)], the intersection constitutes the unique solution of Eq. (11). In the second case [Fig. 2(c)], the straight line

must be tangential to the curve at a point (representing a spinodal) and crosses the curve at a second point, which constitutes the stable solution. In the third case, the central intersection represents an unstable solution whilst the other two are mechanically stable. Among them, the stable (metastable) solution will have the lower (higher) free-energy. If both solutions have the same free-energy, two different thicknesses of adsorbed layer coexist at the wall-fluid interface corresponding to a first order phase boundary [Fig. 2(d)] [27].

- In the limit  $L_1 \rightarrow 0$ , the straight line is vertical and the solution tends to the thickness of the liquid layer adsorbed on the surrounding substrate,  $\ell_1 \rightarrow \ell_2^\pi$ , as expected (see previous subsection). Although the model is not intended to be accurate for very narrow stripes, note that it recovers the correct result in this limit.
- In the limit  $L_1 \rightarrow \infty$ , the straight line is horizontal and the solution recovers the homogeneous substrate,  $\ell_1 \rightarrow \ell_1^\pi$  (see previous subsection).
- If  $\ell_1^\pi = \ell_2^\pi$ , both lines cross at the same point of the horizontal axis and there is only one solution independent of the value  $L_1$  (see previous subsection).
- There is a critical point for a certain combination of the parameters of the problem. This point corresponds to the straight line intersecting the curve tangentially at the point of zero curvature (and negative slope). See Fig. 2(b). Thus, within this approach, a necessary condition for the existence of a critical point is the presence of a point in the effective potential for which the third derivative is zero (the second derivative at that point being negative). This condition can be used to determine a bound for the critical point (see below). Due to the simplicity of the model, the conditions for criticality can be written explicitly as

$$W_1''(\ell_1) = -\frac{2\kappa}{L_1} \quad (12)$$

and

$$W_1'''(\ell_1) = 0, \quad (13)$$

which, together with Eq. (11) determine the critical point completely. Observe that Eqs. (11) and (12) constitute together the conditions for the spinodals.

### C. Second-order Wetting Stripe

To begin we consider the case where the stripe corresponds to a material that exhibits a continuous (critical) wetting transition in the limit of infinite stripe size. No

assumptions about the outer domain have to be made at this moment. Here we concentrate on the most experimentally relevant case of long-ranged forces and write our model effective potential in the usual manner [1]

$$W_1(\ell) = \frac{\Delta T}{\ell^p} + \frac{A}{\ell^{p+1}} + \Delta\mu \delta\rho \ell, \quad (14)$$

where we have rescaled the temperature such  $\Delta T \equiv T - T_w^{(1)}$ ,  $A$  is a (positive) Hamaker constant and  $p$  determines the range of the forces ( $p=2$  for Van der Waals dispersion forces).

The effective potential (14) models the continuous divergence of the film thickness as the temperature is increased towards the wetting temperature  $T_w^{(1)}$  at  $\Delta\mu=0$ . Observe that the third derivative of this potential consists of only two terms and does not depend explicitly on the chemical potential. Recalling the condition for criticality, Eq. (13), it follows that a critical point can only occur provided  $\Delta T < 0$ . In other words, if this system has a critical point, it must occur necessarily at a temperature *below* the wetting temperature  $T_w^{(1)}$ .

The conditions for criticality follow immediately from Eqs. (11) to (13):

$$\ell_{1C} = \left[ \frac{A L_1 (p+1)}{2\kappa} \right]^{\frac{1}{p+3}} \quad (15)$$

$$\Delta T_C = \frac{p+3}{p} \frac{A}{\ell_{1C}} \quad (16)$$

$$\Delta\mu_C \delta\rho = \frac{2\kappa}{L_1} \left( \ell_2^\pi - \frac{p+3}{p+1} \ell_{1C} \right) \quad (17)$$

Figure 3 shows the phase diagram obtained for the effective potential (14) and different values of the stripe width  $L_1$ . For the sake of simplicity, the thickness of the adsorbed layer in the surrounding substrate,  $\ell_2^\pi$ , has been considered constant (independent of the temperature and the chemical potential). This approximation represents a system whose wetting temperature  $T_w^{(2)}$  is higher than the wetting temperature  $T_w^{(1)}$  and for which the variation in the thickness of the adsorbed layer is negligible at temperatures close to  $T_w^{(1)}$ . The advantage of doing is that one can more easily identify the origin of certain features of the surface phase behaviour (see below). The microscopic units of length of the problem are given by  $\lambda \equiv (A/\kappa)^{1/4}$ . In the calculation, we have fixed the range of the forces to be  $p=2$  and the thickness  $\ell_2^\pi = 4\lambda$ . The qualitative features of the phase diagram described here are not in any way specific to these values.

For  $L_1 = 12\lambda$ , the system undergoes an unbending transition represented by a continuous thick line ending

in a critical point (see Fig. 3). Along the line, the adsorbed layer on the stripe can have either of two different thickness, both of them *thinner* than the surrounding adsorbed layer  $\ell_2^\pi$ . Note that the unbending line joins the liquid-vapour coexistence line ( $\Delta\mu = 0$ ) at a certain non-zero angle. This is consistent with Eq. (9) and the fact that the difference in coverage  $\tilde{\Delta}\Gamma \sim \Delta\ell_1$  between the coexisting phases at that point is finite. This transition has been predicted recently [22], although the  $T-\mu$  phase diagram had not been described. Observe that the critical temperature of this transition lies below  $T_w^{(1)}$ , as predicted above. As the stripe width is increased, the length of the unbending line decreases and for a given finite value of the width  $L_1 = L_1^\dagger \approx 53\lambda$ , it vanishes (white circle in Fig. 3). This phenomenology is *identical* to that described for a homogeneous but corrugated substrate [24], showing that the physics involved is essentially the same: the transition takes place due to a balance between the free-energy associated with the direct intermolecular interaction with the substrate and the energetic cost of increasing the area of the liquid-vapour interface. For this particular model, Eq. (14), the transition vanishes for

$$L_1^\dagger = \frac{2\kappa}{A(p+1)} \left( \frac{(p+1)\ell_2^\pi}{p+3} \right)^{p+3} \quad (18)$$

at a temperature

$$\Delta T^\dagger = \frac{(p+3)^2}{p(p+1)} \frac{A}{\ell_2^\pi}. \quad (19)$$

The loci of the critical points are represented in the same figure by a grey thick line. For  $L_1 > L_1^\dagger$ , this line extends further into the metastable region of the phase diagram (dashed grey line) and, in the limit  $L_1 \rightarrow \infty$ , merges asymptotically with the wetting critical point at  $T_w^{(1)}$  (large black circle in Fig. 3). The presence of a (metastable) critical point close to the coexistence line will affect the adsorption properties in the *stable* part of the phase diagram. For instance, the adsorption on the stripe will show a strong increase close to that (metastable) critical point.

The loci of the points for which  $\ell_1^\pi = \ell_2^\pi$  are represented, in the same figure, by a straight black dotted line. Whilst this line does not represent any surface phase transition or singular behaviour, it does significantly influence the possible form of the phase diagram. To see this, recall, as mentioned at the beginning of this section, that the adsorbed layer is flat along that line for *any* value of the stripe width  $L_1$ . Thus, neither the loci of the critical points nor any unbending phase boundary can cross the line  $\ell_1^\pi = \ell_2^\pi$ .

#### D. First-order Wetting Stripe

We now suppose that the stripe corresponds to a material that exhibits a first-order wetting transition in the

limit of infinite stripe size. For this case, we use an effective potential [1]

$$W_1(\ell) = \left( \frac{A^2}{4B} + \Delta T \right) \frac{1}{\ell^p} - \frac{A}{\ell^{p+1}} + \frac{B}{\ell^{p+2}} + \Delta\mu \delta\rho \ell, \quad (20)$$

where  $\Delta T \equiv T - T_w^{(1)}$ ,  $A$  and  $B$  are (positive) Hamaker constants and, as earlier,  $p$  determines the range of the forces. This potential models the discontinuous divergence of the film thickness  $\ell_1^\pi$  at  $T_w^{(1)}$ , and an associated pre-wetting line off coexistence for  $\Delta T > 0$ . This pre-wetting line ends in a pre-wetting critical point ( $\Delta T_{pw}, \Delta\mu_{pw}$ ) where

$$\Delta T_{pw} = \frac{1}{2p(p+3)} \frac{A^2}{B} \quad (21)$$

$$\Delta\mu_{pw} \delta\rho = \frac{2B}{p+1} \left[ \frac{p+1}{2(p+3)} \frac{A}{B} \right]^{p+3}. \quad (22)$$

At this point, the wetting layer thickness is

$$\ell_{pw} = \frac{2(p+3)}{p+1} \frac{B}{A} \quad (23)$$

which will be useful in the following analysis.

A necessary condition for criticality in the finite stripe system is that the effective potential has a point where the third derivative vanishes, (Eq. (13)). This provides an upper bound in temperature for any possible critical point in the system,  $\Delta T_C < 3A^2/(4p(p+4)B)$ . In contrast with the previous case (section III C), a critical point can appear in this system at temperatures above the wetting temperature  $T_w^{(1)}$  (but below a certain threshold). The conditions for the critical point, Eqs. (11)-(13), read

$$(p+1)A\ell_{1C} - 2(p+3)B + \frac{2\kappa}{L_1}\ell_{1C}^{p+4} = 0, \quad (24)$$

$$\Delta T_C = \frac{p+3}{p} \frac{A}{\ell_{1C}} - \frac{(p+3)(p+4)}{p(p+1)} \frac{B}{\ell_{1C}^2} - \frac{A^2}{4B}, \quad (25)$$

and

$$\Delta\mu_C \delta\rho = \frac{2\kappa}{L_1} \left[ \ell_2^\pi - \frac{p+3}{p+1} \ell_{1C} \right] + \frac{2}{p+1} \frac{B}{\ell_{1C}^{p+3}}. \quad (26)$$

In the limit  $L_1 \rightarrow \infty$ , these equations recover (21)-(23), showing that the critical point of the system must merge into the pre-wetting critical point for large stripe widths, as expected (see section III A). Notice that Eq. (24) implies that the thickness at the unbending critical point  $\ell_{1C}$  must be lower than the pre-wetting critical thickness  $\ell_{pw}$  for any finite value of  $L_1$ . This allows us to sharpen our upper bound for the finite stripe width critical temperature to  $T_C < T_{pw}$  for all widths  $L_1$ .

Figures 5-8 show the phase diagrams obtained for the effective potential (20) and different values of the stripe width  $L_1$ . Once again, we have chosen  $\lambda \equiv (A/\kappa)^{1/4}$  as unit of length and the range of the forces has been fixed to  $p = 2$ . Besides, due to the large number of parameters, we have fixed the Hamaker constant  $B = \lambda A$ . As in the previous calculation, the thickness of the adsorbed layer in the surrounding substrate,  $\ell_2^\pi$ , has been considered constant (independent of the temperature and the chemical potential). However, in contrast to the case of critical wetting, different values of  $\ell_2^\pi$  lead to quite different surface phase behaviours. As we shall show, the discriminating parameter here is the ratio of  $\ell_2^\pi$  to  $\ell_{pw}$ .

The phase diagram of this system for  $\ell_2^\pi = 6\lambda$  and  $L_1 = 2000\lambda$  is plotted in Fig. 5. As before, we find a line of first-order unbending phase transitions ending at a critical point (black continuous line). Along this line, phases with distinct adsorptions coexist (see insets). The line  $\ell_1^\pi = \ell_2^\pi$  represents the loci of points for which the adsorbed layer thickness is homogeneous even though the substrate is heterogenous. The line serves to separate interfacial configurations with different convexities [21]. An extension of this line goes beyond the pre-wetting line and joins the coexistence line. Along this extension (long dashed line), the liquid interface is also flat due to the presence of a metastable minimum or even a maximum of the effective potential (20) for  $\ell = \ell_2^\pi$  [28]. Note that this scenario differs from that occurring for a second-order wetting effective potential. In that case, the line  $\ell_1^\pi = \ell_2^\pi$  never hits the coexistence line for any value of the stripe width (see Fig. 3) and, therefore, coexistence *always* takes place between adsorbed layers thinner than the layer adsorbed on the surrounding substrate. In either case, we designate the transition as *unbending* since it originates from the same balance between the energy associated to the interaction with the substrate and the energetic cost of increasing the area of the liquid-vapour interface [22,24].

Observe also in Fig. 5 that the unbending line joins the liquid-vapour coexistence line ( $\Delta\mu=0$ ) at a certain non-zero angle whilst the pre-wetting line approaches that line tangentially. This is due to the fact that the change in the order parameter,  $\ell_1$ , across the unbending transition is *finite* for the unbending transition while is infinite for the pre-wetting transition (because the system is wet for  $T > T_w^{(1)}$  at liquid-vapour coexistence) [see Eq. (9)].

Figure 6 shows the phase diagram of this system for  $\ell_2^\pi = 10\lambda$  and different values of the stripe width  $L_1$ . As  $L_1$  increases, the coexistence line approaches the pre-wetting line. A detailed description of the merging of both lines is given below. Notice the presence of the line  $\ell_1^\pi = \ell_2^\pi$  above the pre-wetting transition and the fact that the unbending transition does not cross that line for any value of  $L_1$ .

The phase diagram for  $\ell_2^\pi = 4\lambda$  and different values of the stripe width  $L_1$  is presented in Fig. 7. As expected, the unbending line merges the pre-wetting line

in the limit  $L_1 \rightarrow \infty$ . Note that the merging is *not* monotonic: as  $L_1$  increases, the unbending line crosses the pre-wetting line and merges from above, close to the coexistence line, and from below, close to the pre-wetting critical point (see inset). The locus of the unbending critical points is similarly non-monotonic for two reasons. On one hand, for small values of  $L_1$ , the unbending transition occurs at  $(\Delta T, \Delta\mu)$  where the potential (20) has only one minimum. Consequently, the loci of the unbending critical points resemble those shown in Fig. 3 for critical wetting. On the other hand, for larger values of  $L_1$ , the unbending transition takes place at  $(\Delta T, \Delta\mu)$  where the potential (20) shows the characteristic double minimum of pre-wetting phase coexistence and the loci of unbending critical point re-routes towards the pre-wetting critical point. The upshot of this is that pre-wetting only has influence on the surface phase diagram for sufficiently large stripe widths  $L_1$ .

The contrast between these mechanisms is clearly magnified for thinner adjacent wetting layers. Fig. 8 shows the phase diagram obtained for  $\ell_2^\pi = \ell_{pw} = 10\lambda/3$ . Observe that the loci of the unbending critical points now cross the liquid-vapour coexistence curve and, for a certain range of width stripes ( $94\lambda \lesssim L_1 \lesssim 938\lambda$ ), the unbending phase transition is not present since it is preempted by bulk condensation. The disappearance of the unbending transition as the stripe width increases (for  $L_1 \approx 93.6\lambda$ ) resembles the behaviour for critical wetting (see Fig. 3). In contrast, when  $L_1 \gtrsim 937.5\lambda$ , the unbending transition *re-enters* the phase diagram (at temperatures above  $T_w^{(1)}$ ) and, in the limit  $L_1 \rightarrow \infty$ , fuses with the pre-wetting line. Notice once more that the behaviour of the unbending line with the stripe width is non-monotonic: after re-entering the phase diagram, its overall position first rises in temperature and, for larger values of  $L_1$ , lowers towards the pre-wetting line (see inset). For the particular effective potential (20), and within the context of the minimal model, this re-entrant behaviour for unbending occurs when

$$\frac{\ell_2^\pi}{\ell_{pw}} < \frac{(p+2)^2}{(p+1)(p+3)}. \quad (27)$$

Observe that the disappearance of the unbending transition (and further re-entry at higher temperatures) for small values of  $\ell_2^\pi$  is inevitable if the unbending transition is not to cross the iso-adsorption line  $\ell_1^\pi = \ell_2^\pi$ , since this line surrounds the pre-wetting critical point as  $\ell_2^\pi$  decreases (see Fig. 4). For this reason, this feature must survive in analysis based on the full interfacial model, Eq. (2).

## E. Discussion

Before we turn to the results for a periodic array of stripes, we complete this section with some critical remarks concerning the features of the phase diagrams pre-

dicted above. To facilitate this, it will be instructive to compare our results with those obtained within the context of the full interfacial model (2), by Bauer and Dietrich (BD) for a particular stripe system made of a material which undergoes a first-order phase transition (when infinite) [21]. Specifically, let us concentrate on the  $T-\mu$  section of the phase diagram shown in Fig. 2 of their article. Whilst their diagram resembles our Fig. 7 in a qualitative way, there are three features which deserve detailed comment:

- In the limit  $L_1 \rightarrow \infty$ , the adsorption characteristics of the stripe must tend to those of the pure substrate, *i.e.* the unbending line must merge with the pre-wetting line. Both approaches capture this requirement, although they differ in the manner in which the mentioned lines coalesce. The main difference lies in the behaviour of the unbending line close to liquid-vapour coexistence. In the BD phase diagram, the unbending line fuses the pre-wetting line monotonically from lower temperatures. In contrast, as described above, the minimal model predicts a non-monotonic merging: close to liquid-vapour coexistence, the unbending line approaches the pre-wetting line from higher temperatures, as  $L_1 \rightarrow \infty$  (see, for example, the inset of Fig. 7).

A detailed calculation with the full interfacial model (2), included in appendix A, shows that either of both situations is possible, and that the actual prevalence of one or the other depends on a number of factors. However, for the experimentally relevant case of dispersion forces,  $p=2$ , we believe the scenario described by the minimal model is the correct one: the unbending line merges with the pre-wetting line from higher temperature *close* to the liquid-vapour coexistence curve. We suspect that numerical problems involved in the large-scale computation of BD are to blame here. For future numerical studies, we note that the behaviour of the unbending line close to coexistence is sensitive to the range of the forces. Consequently, the introduction of a cut-off in the *intermolecular potentials* may well reduce the effective range of the forces, producing a different result for the asymptotic behaviour of the unbending line.

- The intersection of the unbending coexistence line with the bulk liquid-vapour coexistence line is tangential in the BD phase diagram. This feature cannot be correct because the difference in coexisting adsorptions remains finite at  $\Delta\mu=0$ .
- The loci of the unbending critical point in the BD phase diagram show a nontrivial behaviour as a function of the stripe width  $L_1$ . That behaviour is analogous to that of Fig. 7 and is explained above in terms of unbending in the presence or absence of energetic barrier in the effective potential  $W_1$ .

However, the BD phase diagram shows that, additionally, for even smaller values of the stripe width, the loci of unbending critical points curve towards the liquid-vapour coexistence line. To explain that, we note that the minimal model prediction for the critical temperature, Eq. (25), does *not* depend on the thickness of the adsorbed layer on the surrounding substrate  $\ell_2^\pi$ , while the critical chemical potential, Eq. (26), does (in fact, in very simple manner). The curving of the loci of unbending critical points towards the liquid-vapour coexistence line for very narrow stripes, found by BD, is therefore a direct consequence of the *thinning* of the adsorbed layer on the surrounding substrate. This illustrates the merit of first keeping the value of  $\ell_2^\pi$  constant before allowing for its own dependence on temperature and chemical potential.

## IV. PERIODIC STRIPES

### A. General Considerations

Consider next a periodic array of stripes made of two different materials (Fig. 1(b)) whose adsorption properties can be described, when pure, by the effective potentials  $W_1(\ell)$  and  $W_2(\ell)$ , respectively. The widths of the stripes are denoted  $L_1$  and  $L_2$ , and the period  $L=L_1+L_2$ . This system can be considered as the simplest prototype for studying heterogenous wetting since for a single stripe the wetting properties are completely determined by the embedding material. Thus, the periodic system can be used to study the dependence of the wetting temperature on different factors such as composition, degree of domain separation, etc. This has already been done to a certain degree within density functional theory [14], but this approach seems more suitable to study packing phenomena close to the heterogeneities of the surface. As regards the global wetting properties, we believe that a simpler approach will suffice. This system has also been studied experimentally [4], mainly in the context of contact angles and Cassie's empirical law [29]. This law states that the contact angle  $\theta$  of a macroscopic drop placed on a planar heterogeneous substrate satisfies

$$\cos \theta = \sum_i \gamma_i \cos \theta_i, \quad (28)$$

where  $\theta_i$  is the contact angle of a droplet on a (pure) material of type  $i$ , and  $\gamma_i$  is the fractional area of the substrate made of that material. The implication of this law for the wetting temperature of a heterogeneous system is straightforward:

$$T_w = \max\{T_w^{(1)}, T_w^{(2)}, \dots\}, \quad (29)$$

where  $T_w^{(i)}$  is the wetting temperature of the substrate  $i$  (when pure). Here we check the validity of this law with

the help of the minimal model put forward in section II. First, however, we recall briefly some general considerations concerning this system:

- For any given period  $L$ , the limiting cases  $L_1 \rightarrow 0$  and  $L_2 \rightarrow 0$  must produce the pure systems 1 and 2, respectively. This fact follows trivially from the Hamiltonian (5). Observe, however, that it contradicts clearly Cassie's law since Eq. (29) states that infinitesimal amounts of a substance can change the wetting properties of the embedding substrate.
- If the thickness of the adsorbed layers on both infinite substrates is the same ( $\ell_1^\pi = \ell_2^\pi$ ), the functional (2) is fully minimised, term by term, by a flat solution  $\ell(x) = \ell_1^\pi = \ell_2^\pi$ , as in the single stripe system. For that reason, the loci of the points for which  $\ell_1^\pi = \ell_2^\pi$  are not to be crossed by any surface phase coexistence line. These are homogeneous states on a heterogeneous substrate. Note that since both  $\ell_1^\pi$  and  $\ell_2^\pi$  vary with the temperature and chemical potential, the loci of the points for which  $\ell_1^\pi = \ell_2^\pi$  may not be simple in the  $T - \mu$  plane. Indeed, the line may not exist at all.
- If an unbending first-order transition takes place between different surface phases, the coexistence line in the  $T - \mu$  plane will verify the Clausius-Clapeyron-like equations (8) and (9).

## B. Minimal Model

As described in section II, the free-energy of this system is given, within the minimal model prescription, by the two-variable function  $H(\ell_1, \ell_2)$ , Eq. (5). This free-energy depends on the *average* thicknesses  $\ell_1$  and  $\ell_2$ , whose equilibrium value, for a given temperature and chemical potential, is determined by minimisation of the free-energy. This yields the following coupled equations:

$$\begin{aligned} 2\kappa(\ell_1 - \ell_2) + L_1 W_1'(\ell_1) &= 0 \\ 2\kappa(\ell_2 - \ell_1) + L_2 W_2'(\ell_2) &= 0. \end{aligned} \quad (30)$$

Adding both equations we obtain the *sum rule*

$$L_1 W_1'(\ell_1) + L_2 W_2'(\ell_2) = 0, \quad (31)$$

which is the counterpart of another, obtained with the full interfacial model (2)

$$\int_{\mathcal{L}_1} dx W_1'(\ell) + \int_{\mathcal{L}_2} dx W_2'(\ell) = 0. \quad (32)$$

Eqns. (30) can be solved by means of a graphical construction. The solution corresponds to the intersection of the curves

$$\begin{aligned} \ell_2 &= \ell_1 + \frac{L_1}{2\kappa} W_1'(\ell_1) \\ \ell_1 &= \ell_2 + \frac{L_2}{2\kappa} W_2'(\ell_2), \end{aligned} \quad (33)$$

in the  $\ell_1 - \ell_2$  plane, as seen in Fig. 9. As before, if there are multiple solutions, the stable one can be discriminated upon comparison of their free-energies, Eq. (5).

Among these solutions, it is straightforward to identify the spinodal points since they occur when the two curves of the graphical construction are tangential to each other at a given point. This leads to the following equation

$$\left(1 + \frac{L_1}{2\kappa} W_1'(\ell_1)\right) \left(1 + \frac{L_2}{2\kappa} W_2'(\ell_2)\right) = 1, \quad (34)$$

which can be obtained, alternatively, from the vanishing of the determinant of the Hessian of the free-energy  $H(\ell_1, \ell_2)$ . In addition, possible critical points can occur if (34) is satisfied at a point of inflexion on any of the curves:

$$\begin{aligned} W_1'''(\ell_1) &= 0 \\ \text{or} \\ W_2'''(\ell_2) &= 0. \end{aligned} \quad (35)$$

The existence of *two* alternative conditions for the presence of a critical point suggests that, in principle, there could be *two* different critical points in the  $T - \mu$  phase diagram. This is quite different to that obtained for the single stripe system. In particular, as the limiting cases  $L_2 = 0$  and  $L_1 = 0$  are each associated with one of the equations (35), it follows that there must be *two* unbending coexistence lines which, in principle, could occur simultaneously in the  $T - \mu$  phase diagram. All these features, which emerge naturally from only elementary considerations of the minimal model, would be much more difficult to extract from the full interfacial description (2).

## C. Cassie's Law

Before applying the model to some specific examples, we make connection between Cassie's law and the minimal model. To do that, we define the fractional area of material 1 as  $\gamma \equiv L_1/L$  for a given period  $L$ . This allows us to write the free-energy of the system per unit length in the following way

$$h(\ell_1, \ell_2) = \frac{\kappa}{L} (\ell_1 - \ell_2)^2 + \gamma W_1(\ell_1) + (1 - \gamma) W_2(\ell_2), \quad (36)$$

which, in turn, enables us to change from a description in terms of  $L_1$  and  $L_2$  into another in terms of  $L$  and  $\gamma$ . In this latter case,  $L$  can be understood as a measure of the overall size of the stripes, while  $\gamma$  will be the fractional



area of material 1. This is obviously true as long as  $\gamma$  is not too close to the limiting cases  $\gamma=0$  and  $\gamma=1$ . These limiting cases give rise (trivially) to the pure substrates 2 and 1, respectively (for any value of the period  $L$ ).

Consider now, that the period  $L$  is very large. This represents systems for which the heterogeneities extend over macroscopic areas. In this case, we can neglect the first term of (36) and, consequently, the variables  $\ell_1$  and  $\ell_2$  decouple. Minimisation of the energy is achieved by  $\ell_1 = \ell_1^\pi$  and  $\ell_2 = \ell_2^\pi$  and the free-energy of the system,  $\omega(T, \mu) \equiv \min h$ , can be approximated

$$\omega(T, \mu) \approx \gamma W_1(\ell_1^\pi) + (1-\gamma) W_2(\ell_2^\pi), \quad (37)$$

which is but a different way of writing Cassie's law, Eq. (28), as generally accepted. The minimal model, therefore, recovers Cassie's phenomenological law in the limit of macroscopic heterogeneities.

The other limiting case, corresponding to small values of  $L$ , represents systems for which the heterogeneities are of microscopic size. These systems are quasi-homogenous since the two materials are closely intermingled on the surface. Recall that our model was not intended to work under these assumptions. In spite of this, the limit  $L \rightarrow 0$  produces a sensible result. This occurs because the first term of the free-energy (36) becomes exceptionally important and has to be minimized fully yielding  $\ell_1 = \ell_2$ ; *i.e.* the thickness of the adsorbed layer is approximately the same at every point of the substrate. The system behaves, in this limit, as a homogeneous system whose adsorption properties will be given by the following *averaged* effective potential

$$\overline{W}(\ell) \equiv \gamma W_1(\ell) + (1-\gamma) W_2(\ell). \quad (38)$$

This description tallies with the spirit of the construction of the effective potentials as an integral of the solid-liquid and liquid-liquid interactions over the entire system [30].

Therefore, the minimal model seems to describe the behaviour of the heterogenous system in the two mentioned limits (macroscopic and microscopic heterogeneities) in a physical way. We are fully aware of the fact that such a broad description is achieved by smearing out some subtle details, and that the model will not work under certain special circumstances. Nevertheless, we stress that the model is put forward just as a versatile approximation to the full effective interfacial description, Eq. (1).

#### D. Examples

As suggested above, we expect a very rich behaviour in the periodic system of parallel stripes. A full exploration of the phenomenology of this system is a colossal task, well beyond the scope of this paper. Therefore, we only report here the calculation of the wetting temperature for two heterogeneous systems as an example of the method.

We consider substrates undergoing first-order wetting transitions (when pure), whose effective potentials will be modelled by

$$W_1(\ell) = \left( \frac{A_1^2}{4B_1} + (T - T_w^{(1)}) \right) \frac{1}{\ell^p} - \frac{A_1}{\ell^{p+1}} + \frac{B_1}{\ell^{p+2}}, \quad (39)$$

and

$$W_2(\ell) = \left( \frac{A_2^2}{4B_2} + \alpha(T - T_w^{(2)}) \right) \frac{1}{\ell^p} - \frac{A_2}{\ell^{p+1}} + \frac{B_2}{\ell^{p+2}}, \quad (40)$$

Out of bulk liquid-vapour coexistence, the usual term  $\Delta\mu \delta\rho \ell$  must be added, although we do not consider this possibility here. The parameters  $A_1$ ,  $B_1$ ,  $A_2$ , and  $B_2$  are (positive) Hamaker constants characterising the pertinent potentials. Notice that a dimensionless constant  $\alpha$  has to be included (multiplying the temperature in  $W_2(\ell)$ ) to account for differences in surface entropy between the two pure systems. We use  $\lambda \equiv (A_1/\kappa)^{1/4}$  as unit of length.

From this vast space of parameters we have chosen two examples, both for long-range (dispersion) forces,  $p = 2$ . For each of them, we have calculated the wetting temperature of the periodic system as a function of the fractional area of material 1,  $\gamma$ , for different values of the period  $L$ . As mentioned above, the modification of the wetting temperature with the composition of the substrate constitute a distinctive and important characteristic of these periodic systems since, for a single stripe, the wetting temperature is necessarily determined by the (infinitely wide) abutting substrate. The results, for different choices of parameters, are shown in Figs. 10 and 11.

Let us concentrate first on Fig. 10. As expected, the wetting temperature ranges between  $T_w^{(2)}$  (for  $\gamma=0$ ) and  $T_w^{(1)}$  (for  $\gamma=1$ ), independently of the value of the period  $L$ . For small periods, the wetting temperature interpolates almost linearly between  $T_w^{(2)}$  and  $T_w^{(1)}$  (as a function of  $\gamma$ ). This linearity is merely fortuitous. In general,  $T_w(\gamma)$  will be a non-linear function joining the limiting cases  $T_w^{(2)}$  and  $T_w^{(1)}$ . Within the minimal model, the wetting temperature of the heterogeneous system can be calculated, in this limit  $L \rightarrow 0$ , as the wetting temperature of the averaged potential  $\overline{W}(\ell)$ , Eq. (38). More specifically, for the model effective potentials (39) and (40), we can write an analytical expression for the wetting temperature in the mentioned limit

$$T_w(\gamma) = \frac{\gamma T_w^{(1)} + \alpha(1-\gamma) T_w^{(2)}}{\gamma + \alpha(1-\gamma)} - \frac{\gamma(1-\gamma)(A_1 B_2 - A_2 B_1)^2}{(\gamma + \alpha(1-\gamma)) B_1 B_2 (\gamma B_1 + (1-\gamma) B_2)}, \quad (41)$$

which is clearly non-linear.

As the period is increased, Cassie's law, Eq. (29), is recovered and  $T_w(\gamma) \approx T_w^{(1)} > T_w^{(2)}$ , for almost every value of the fractional area  $\gamma$ . Deviations occur only for small  $\gamma$ . These deviations become progressively less important for large periods  $L$ , as expected.

The same quantity, calculated for a different system, is plotted in Fig. 11. In this case, the differences between substrates 1 and 2 are stonger: the thicknesses of the adsorbed layers on the pure substrates become very dissimilar for temperatures  $T \lesssim T_w^{(2)}$  and so do their interfacial tensions (free-energies). In particular, the adsorbed layer on substrate 1 is (in general) thicker than the corresponding layer of substrate 2 (see Fig. 12) and its free energy is lower. This introduces new phenomenology in the phase behaviour. For small periods,  $L = 0.1\lambda$ , the wetting temperature of the periodic system resembles an *inversed* Cassie's law since  $T_w(\gamma) \approx T_w^{(2)} < T_w^{(1)}$ , for most values of the fractional area  $\gamma$ . The fact that the adsorption properties of the substrates differ considerably appears to have a decisive influence on the adsorption properties of the system in the quasi-homogeneous limit,  $L \rightarrow 0$ . As we increase the value of  $L$ , we begin to recover the behaviour dictated by Cassie's law. On route to this, however, we uncover unexpected richness. For the parameters used here, this first occurs for  $L \gtrsim 0.2\lambda$ , and is clearly visible for  $L = 1.0\lambda$ . The broken line in Fig. 11 corresponds to a (first-order) unbending transition where adsorbed layers of different thicknesses coexist (similar to those occurring for a single heterogeneous stripe). This coexistence finishes at an unbending critical point (represented by a black circle) as it did in the single stripe system. Of course, in the periodic system, the unbending phase transition is associated with an adsorption jump on both domains. Fig. 12 shows the thicknesses of the adsorbed layers  $\ell_1$  and  $\ell_2$  on substrates 1 and 2, respectively, as a function of the temperature for a particular system ( $L = 10\lambda$ ,  $\gamma = 0.1$ ) corresponding to those wetting temperatures plotted in Fig. 11. The thickness of the layers adsorbed on the pure substrates  $\ell_1^\pi$  and  $\ell_2^\pi$  are also shown for the sake of comparison. Observe that for  $(T - T_w^{(1)})\lambda/A_1 > -0.02$  the liquid interface has unbent and is essentially flat ( $\ell_1 \approx \ell_2$ ). Bearing this in mind, we refer to the phase diagrams of Fig. 11 and notice (for instance, for  $L = 1.0\lambda$  or  $10\lambda$ ) that the presence of the unbending transition modifies the qualitative shape of curve representing the wetting temperature  $T_w(\gamma)$ . Specifically, at the point where the unbending transition merges with the curve  $T_w(\gamma)$ , the latter has a kink. At the right of that point,  $T_w(\gamma)$  grows with a slope similar to the slope of the unbending coexistence line, and tends to  $T_w^{(1)}$  very rapidly (as a function of  $\gamma$ ). We can interpret this as an unbending-mediated wetting transition. In other words, at  $T_w(\gamma)$  the interface unbends to the wet configuration  $\ell_1 = \ell_2 = \infty$ . On the other hand, to the left of that merging point, the interface finds a stable (unbent) flatter configuration ( $\ell_1 \approx \ell_2$ ) resembling those of the quasi-homogeneous limit ( $L \approx 0$ ). Observe that  $T_w(\gamma)$  hardly

changes by increasing  $L$  in that region of the phase diagram from the curve obtained for  $L = 0.1\lambda$ . This region, and the unbending line, are squeezed towards small values of the fractional area  $\gamma$  for larger values of the period  $L$ . Notice that the unbending line can neither disappear (because that limit contains the unbending transition for the single stripe line) nor merge with the line  $\gamma = 0$  (representing pure substrate 2, which does not undergo any unbending transition). However, it becomes progressively and proportionally less important as  $L$  grows and remains confined to the region of small fractional area,  $\gamma \approx 0$ . In the limit of macroscopic heterogeneities,  $L \rightarrow \infty$ , Cassie's law is recovered as discussed earlier.

## V. CONCLUSIONS

In this paper, we have forwarded a simple model of surface phase behaviour for fluid adsorption on heterogeneous micropatterned substrates. This has been applied to two proto-typical systems: a) a single stripe of a material exhibiting either a first- or second-order wetting transition embedded in an infinite partially wet substrate and b) a periodic array of stripes each of which exhibit first-order wetting at distinct temperatures. The advantage of our "minimal" description is that it allows us to explore the vast phase space of parameters that these systems present. This would be an extremely arduous task within even an effective interfacial Hamiltonian description, let alone a microscopic density functional approach. Despite the simplicity of our model, we rederive results obtained previously using more microscopic methods for specific choices of interfacial binding potentials. This gives us confidence concerning the validity of our method. Applying the minimal model to other choices of substrate heterogeneity, we predict new examples of surface phase behaviour. In particular, for the single stripe system with first-order wetting, we establish the conditions under which the unbending coexistence line approaches the pre-wetting line (of the pure substrate) from above or below, in the limit of large stripe widths. For the periodic system, we have concentrated on establishing the value of the wetting transition temperature as a function of the fractional area of the two materials as well as the total period of the heterogeneity. Agreement with Cassie's empirical law is obtained in the limit of macroscopically large domain sizes. Thus, the wetting temperature of the heterogeneous substrate is essentially determined by the maximum wetting temperature of each of the pure components. For mesoscopic systems, on the other hand, notable deviations from Cassie's law are possible. This includes "inversions" of Cassie's law where we observe that the wetting temperature of the heterogeneous substrate is close to the lower of the two wetting temperatures of the pure components. The value of the wetting temperature may also be sensitive to the presence of unbending phase transitions induced by the heteroge-

neous substrate. It is clear to us that even within the context of the present minimal description, the possible surface phase behaviour on the periodic micropatterned substrate is extraordinarily rich. For example, out of bulk two phase coexistence, additional phenomenology may arise due to the competition between lengthscales associated with the pre-wetting line on each pure component. A full exploration of the possible surface phase behaviour requires much further work along these lines.

We are very grateful to Prof. M.E. Cates for support during the completion of this project. C.R. acknowledges economical support from the E.C. under contract ERBFMBICT983229.

\* Present address: Dept. of Physics and Astronomy, University of Edinburgh, Edinburgh EH9 3JZ, United Kingdom.

## APPENDIX A:

Consider an infinite stripe of width  $L_1$  made of material 1 that is embedded in a substrate made of material 2 (Fig. 1(a)). If these materials are such that their adsorption properties can be described (when pure) by effective potentials  $W_1$  and  $W_2$ , the adsorption properties of the combined system can be obtained by the functional minimisation of the free-energy (2). If substrate 1 undergoes a first-order wetting transition at  $T = T_w^{(1)}$  when pure (and, therefore, its phase diagram presents a pre-wetting line), the combined system must undergo an unbending transition whose coexistence line must merge with the pre-wetting line of the pure substrate in the limit  $L_1 \rightarrow \infty$  (as explained in the main text of the paper).

In this appendix, we want to determine under which circumstances the interfacial model (2) predicts that, in the mentioned limit  $L_1 \rightarrow \infty$ , the unbending line approaches the pre-wetting line from above or from below (*i.e.* from temperatures higher or lower than the wetting temperature  $T_w^{(1)}$ , respectively). We denote these two possibilities as scenarios A (above) and B (below). As we are mainly interested in the merging of the two lines close to the bulk liquid-vapour coexistence line (see III E), we only need to concentrate on  $\Delta\mu = 0$ .

To start, we notice that our goal can be achieved, without lack of generality, by studying the system at the wetting point  $T = T_w^{(1)}$ . Scenario A will be correct if the stable configuration, at that point, corresponds to a bound state in the limit  $L_1 \rightarrow \infty$ . On the other hand, if the stable configuration is unbound in that limit, the scenario B will be followed. In other words, for  $T = T_w^{(1)}$  and  $\Delta\mu = 0$ , there must be two different configurations which minimise the Hamiltonian (2) in the limit  $L_1 \rightarrow \infty$  (see below). This occurs due to the presence of a local maxima (the activation barrier) in the potential  $W_1(\ell)$

at the wetting point. We denote these configurations by  $\ell^-(x)$  (bound) and  $\ell^+(x)$  (near-unbound). If  $\ell^-(x)$  is the stable configuration (it has lower energy), scenario A will be correct. Otherwise, it will be scenario B.

Minimization of (2) yields the following Euler-Lagrange equation:

$$\Sigma \ddot{\ell}(x) = \begin{cases} W_1'(\ell) & \text{if } |x| \leq L_1/2 \\ W_2'(\ell) & \text{if } |x| > L_1/2, \end{cases} \quad (\text{A1})$$

where we have located the origin  $x = 0$  in the center of the stripe. This equation can be integrated once to yield:

$$\frac{\Sigma}{2} \dot{\ell}(x)^2 = \begin{cases} \Delta W_1(\ell) - \mathcal{P} & \text{if } |x| \leq L_1/2 \\ \Delta W_2(\ell) & \text{if } |x| > L_1/2, \end{cases} \quad (\text{A2})$$

where  $\Delta W_1(\ell) \equiv W_1(\ell) - W_1(\ell_1^\pi)$ ,  $\Delta W_2(\ell) \equiv W_2(\ell) - W_2(\ell_2^\pi)$ , and  $\mathcal{P}$  is a (non-negative) constant of integration to be determined. Note that the boundary condition at  $x = \infty$  has been imposed. Further conditions read

$$\begin{aligned} \Delta W_1(\ell_0) &= \mathcal{P} \\ \Delta W_1(\ell_L) &= \Delta W_2(\ell_L) + \mathcal{P}, \end{aligned} \quad (\text{A3})$$

where  $\ell_0 \equiv \ell(0)$  and  $\ell_L \equiv \ell(L_1/2)$ . These two equations can be solved by means of a geometrical construction for an arbitrary value of  $\mathcal{P}$  (see Fig. 13). The relevant value for our case (the limit  $L_1 \rightarrow \infty$ ) is  $\mathcal{P} \rightarrow 0$  (see below). Notice in the figure that the different pairs of values  $\ell_0^-$ ,  $\ell_L^-$  and  $\ell_0^+$ ,  $\ell_L^+$  will give rise to the two solutions  $\ell^-(x)$  and  $\ell^+(x)$ .

Here we can make our first prediction with the help of the geometrical construction: if  $\ell_1^\pi \geq \ell_2^\pi$ , the correct scenario must be A for any physical shape of the effective potentials  $W_1$  and  $W_2$ . This happens because, under these circumstances, *every* term of the Hamiltonian turns out to be lower for the bound configuration  $\ell^-(x)$  than for the near-unbound one (if the latter exists at all). This (purely geometrical) feature is captured correctly by the minimal model (6). However, if  $\ell_1^\pi < \ell_2^\pi$  at the wetting point, the two configurations exist (in this case  $\ell^+(x)$  always exists for sufficiently large values of  $L_1$ ) and their free-energies need to be calculated.

To proceed, we use equation (A2) to write the quadrature

$$L_1 = \sqrt{2\Sigma} \left| \int_{\ell_0}^{\ell_L} \frac{dx}{\sqrt{\Delta W_1(\ell) - \mathcal{P}}} \right|, \quad (\text{A4})$$

which determines  $\mathcal{P}$  implicitly as a function of the stripe width  $L_1$ ,  $T$  and  $\mu$ . A simple calculation shows that  $\mathcal{P}$  is related to the free-energy of the system in the following way:

$$\mathcal{P} = \frac{\partial \omega}{\partial L_1} + W_2(\ell_2^\pi) - W_1(\ell_1^\pi). \quad (\text{A5})$$

Thus, the comparison of the energies of configurations  $\ell^-(x)$  and  $\ell^+(x)$  can be obtained from the asymptotic behaviour of  $\mathcal{P}$  for large values of  $L_1$ . In turn, this follows from studying the asymptotic behaviour of (A4) when  $\mathcal{P} \rightarrow 0$ , since this is the only value for which the integral diverges and recovers, in that way, the limit  $L_1 \rightarrow \infty$ . For appropriate effective potentials  $W_1$  and  $W_2$  (with the only requirement that  $W_1$  has an activation barrier), we obtain

$$\begin{aligned} \mathcal{P}^- &\sim L_1^{-4} \\ \mathcal{P}^+ &\sim L_1^{-\frac{2p}{p+3}}, \end{aligned} \quad (\text{A6})$$

where  $(-)$  and  $(+)$  denote the bound and near-unbound configuration, respectively, and  $p$  is the range of the forces, *i.e.*  $W_1(\ell) \sim \ell^{-p}$  when  $\ell \rightarrow \infty$ . Therefore, the energy of each configuration can be written asymptotically as

$$\begin{aligned} \omega^- &\sim \omega_0^- + \omega_1^- L_1^{-3} + \dots \\ \omega^+ &\sim \omega_0^+ + \omega_1^+ L_1^{\frac{3-p}{p+3}} + \dots, \end{aligned} \quad (\text{A7})$$

where  $\omega_0^-$ ,  $\omega_0^+$ ,  $\omega_1^-$  and  $\omega_1^+$  are constants that depend on the details of the potential. Note that the irrelevant common term  $[W_2(\ell_2^\pi) - W_1(\ell_1^\pi)] L_1$  has been subtracted.

Consequently, the range of the forces  $p$  appears to be determinant in establishing which of the two scenarios holds. For  $p < 3$ , the energy of the bound configuration tends to a constant for large stripe widths,  $\omega^- \rightarrow \omega_0^-$ , while the energy of the near-unbound configuration diverges as a function of the stripe width  $L_1$ . For that reason, the bound configuration  $\ell^-(x)$  is the stable one in this case, and scenario A is correct. This includes the experimentally relevant case of dispersion forces,  $p = 2$ . In contrast, for  $p \geq 3$ , both  $\omega^-$  and  $\omega^+$  tend to constant values in the limit  $L_1 \rightarrow \infty$ . The prevalence of scenario A or B will be determined, in this latter case, by the comparison of the free-energies:

$$\frac{\omega_0^-}{2\sqrt{2\Sigma}} = \int_{\ell_1^\pi}^{\ell_L} d\ell \sqrt{\Delta W_1(\ell)} + \int_{\ell_L}^{\ell_2^\pi} d\ell \sqrt{\Delta W_2(\ell)}, \quad (\text{A8})$$

and

$$\frac{\omega_0^+}{2\sqrt{2\Sigma}} = \int_{\ell_L}^{\infty} d\ell \sqrt{\Delta W_1(\ell)} + \int_{\ell_2^\pi}^{\ell_L} d\ell \sqrt{\Delta W_2(\ell)}. \quad (\text{A9})$$

The necessary conditions for scenarios A or B to occur are gathered in the following table:

Conditions		Scenario	
$\ell_1^\pi \geq \ell_2^\pi$		A	
$\ell_1^\pi < \ell_2^\pi$	$p < 3$	A	
	$p \geq 3$	$\omega_0^- < \omega_0^+$	A
		$\omega_0^- > \omega_0^+$	B

where  $\ell_1^\pi$  and  $\ell_2^\pi$  are the wetting layer thicknesses on the pure substrates measured at  $T = T_w^{(1)}$ .

- 
- [1] For a review, see, for example, S. Dietrich, in "Phase Transitions and Critical Phenomena", (C. Domb and J.L. Lebowitz, eds.), Vol. **12**, p. 1 (Academic Press, London, 1988).
- [2] See, for example, B. H. Weigl, P. Yager, Science **283**, 346 (1999). See also the collected papers J. Micromech. Microeng. **4**, n. 4 (1994).
- [3] C. Rascón and A.O. Parry, Nature **407**, 986 (2000).
- [4] J. Drelich *et al.*, Langmuir **12**, 1913 (1996).
- [5] P.S. Swain and R. Lipowsky, Langmuir **14**, 6772 (1998).
- [6] J.T. Woodward, H. Gwin and D.K. Schwartz, Langmuir **16**, 2957 (2000).
- [7] M.H. Adão *et al.*, Phys. Rev. E **59**, 746 (1999).
- [8] P. Lenz and R. Lipowsky, Phys. Rev. Lett. **80**, 1920 (1998).
- [9] C. Bauer and S. Dietrich, Eur. Phys. J. B **10**, 767 (1999).
- [10] D. Urban, K. Topolski and J. de Coninck, Phys. Rev. Lett. **76**, 4388 (1996).
- [11] J.R. Henderson, Mol. Phys. **98**, 677 (2000).
- [12] A.O. Parry, E.D. Macdonald and C. Rascón, J. Phys.: Condens. Matter. (to appear), cond-mat/0008036.
- [13] S. Palacin *et al.*, Chem. Matter. **8**, 1316 (1996).
- [14] L.J. Douglas Frink and A.G. Salinger, J. Chem. Phys. **110**, 5969 (1999).
- [15] H. Gau *et al.*, Science **283**, 46 (1999).
- [16] M. Böltau *et al.*, Nature **391**, 877 (1998).
- [17] A. Karim *et al.*, Phys. Rev. E **57**, R6273 (1998).
- [18] K. Kargupta, R. Konnur and A. Sharma, Langmuir **16**, 10243 (2000).
- [19] C. Bauer and S. Dietrich, Phys. Rev. E **60**, 6019 (1999).
- [20] C. Bauer, S. Dietrich and A.O. Parry, Europhys. Lett., **47** 474 (1999).
- [21] C. Bauer and S. Dietrich, Phys. Rev. E **61**, 1664 (2000).
- [22] C. Rascón and A.O. Parry, J. Phys.: Condens. Matter., **12** A369 (2000).
- [23] Details about effective potentials can be found in [1].
- [24] C. Rascón, A.O. Parry and A. Sartori, Phys. Rev. E **59**, 5697 (1999).
- [25] The structure of such near-flat profiles beyond the interfacial model (2), is discussed in ref. [21].
- [26] E.H. Hauge and M. Schick, Phys. Rev. B **27**, 4288 (1983).
- [27] Standard finite-size scaling theory predicts that fluctuation effects, beyond the present mean-field consideration, modify this to a sharply rounded pseudo-first-order phase transition. For details, see ref. [20].
- [28] The possibility of using a maximum of the effective potential to stabilise a solution is discussed in [22].
- [29] A.B.D. Cassie, Discuss. Faraday Soc. **3**, 11 (1948).
- [30] J. Israelachvili, *Intermolecular & Surface Forces* (Academic, London, 1991).

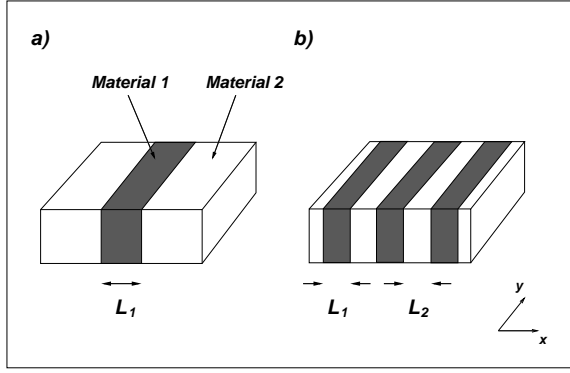


FIG. 1. Schematic illustration of micropatterned substrates considered in this paper. The figure shows a) a single stripe of width  $L_1$  embedded in substrate 2 and b) a periodic array of stripes of widths  $L_1$  and  $L_2$ , made of materials 1 and 2, respectively. Both systems are translationally invariant along the  $y$  direction.

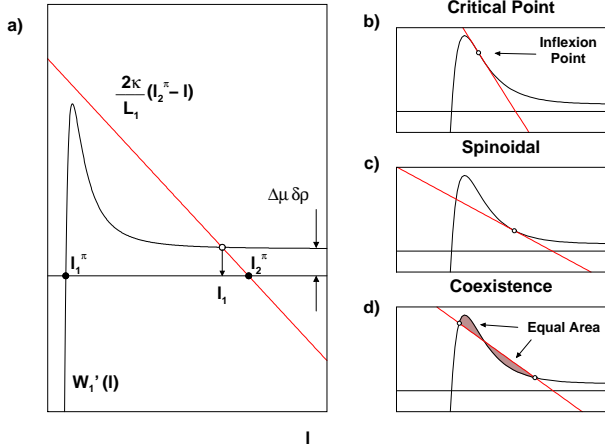


FIG. 2. Sketch of the graphical construction used to solve Eq. (11). The *average* thickness of the adsorbed layer on the stripe,  $\ell_1$ , is obtained by the intersection of the curve  $W_1'(\ell)$  with the straight line  $2\kappa(\ell_2^\pi - \ell)/L_1$  (see (a)). The geometrical conditions for a critical point (b), a spinodal (c), and the coexistence between two different values of the adsorption  $\ell_1$  (d) are also shown.

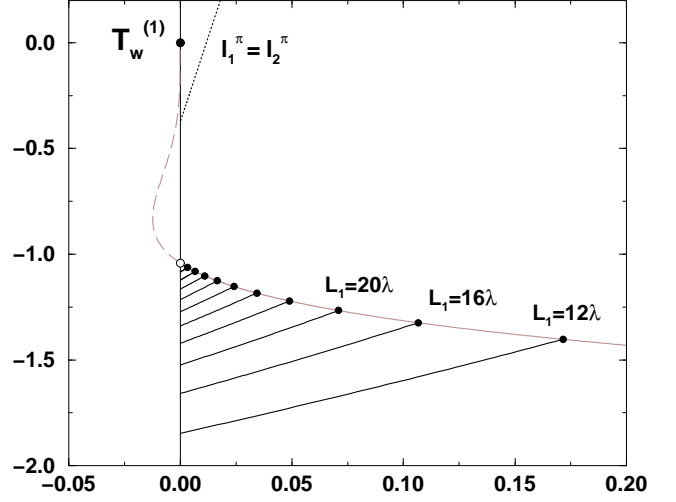


FIG. 3.  $T-\mu$  phase diagram for the adsorption on a stripe of different widths  $L_1$ . The stripe is made of a material that, when pure, undergoes a *second-order* wetting transition at  $T = T_w^{(1)}$  (large full circle), whose adsorption properties are described by the effective potential (14). The stripe is embedded in a partially wet substrate with finite film thickness  $\ell_2^\pi = 4\lambda$ . This system shows an *unbending* transition (black continuous lines) for a range of stripe widths. In the figure,  $L_1/\lambda = 12, 16, 20, 24, 28, 32, 36, 40, 44$  and  $48$ . For  $L_1 \approx 53\lambda$ , the unbending transition is pre-empted by the bulk liquid-vapour phase transition (large empty circle). The continuous grey line represents the loci of the critical points (as given by Eqs. (15-17)). This line extends into the metastable region of the phase diagram (dashed grey line) and tends asymptotically to the wetting temperature  $T_w^{(1)}$  when  $L_1 \rightarrow \infty$ . Note that the unbending transition does *not* cross the iso-adsorption line  $\ell_1^\pi = \ell_2^\pi$ , (dotted line).

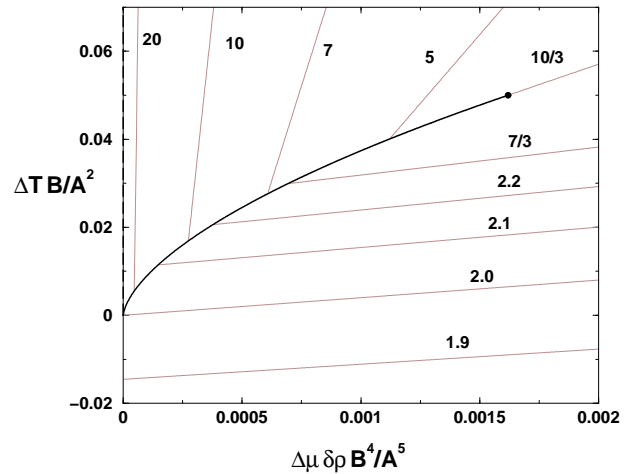


FIG. 4. pre-wetting line (black) as modelled by the effective potential (20) with  $p=2$ . Iso-adsorption lines (grey) are also shown for different values of the adsorption  $\ell$  ranging between 1.9 and 20 (in units of  $B/A$ ).

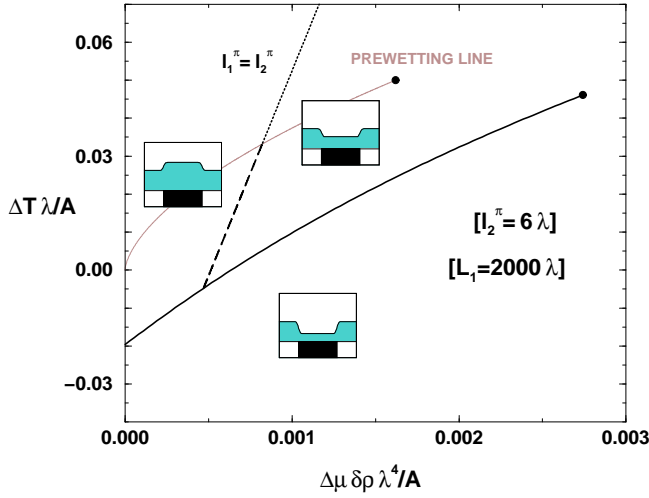


FIG. 5.  $T-\mu$  phase diagram for the adsorption on a stripe of width  $L_1$  made of a material exhibiting a *first-order* wetting transition (when pure). The stripe is embedded in a partially wet substrate whose wetting layer thickness  $\ell_2^\pi$  is considered independent of temperature and chemical potential. The pre-wetting line of the (pure) material 1 is shown for comparison (See text for details).

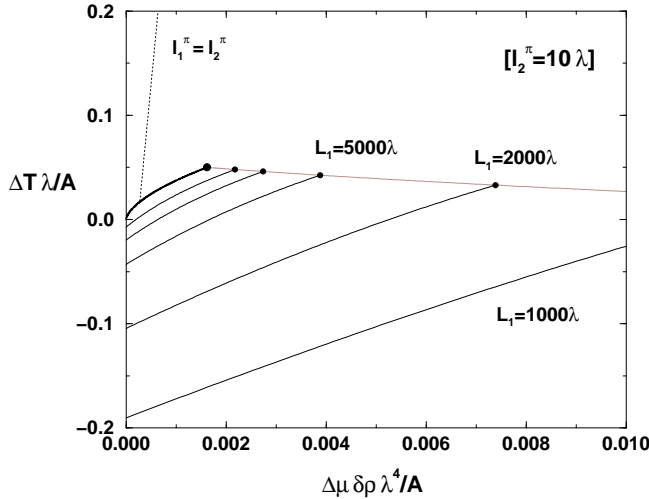


FIG. 6.  $T-\mu$  phase diagram showing unbending phase transitions occurring on a substrate with a single stripe showing a *first-order* wetting transition (when pure), embedded in a substrate whose wetting layer thickness  $\ell_2^\pi = 10\lambda$ . The unbending coexistence lines are represented by thin black lines which finish at critical points, the loci of which is shown as grey. Different stripe widths are considered:  $L_1 = 1, 2, 5, 10$  and  $20 (\times 10^3\lambda)$ . The pre-wetting line of the (pure) material 1, which corresponds to the unbending line in the limit  $L_1 \rightarrow \infty$ , is shown for comparison (thick line). The broken line represents the line for which  $\ell_1^\pi = \ell_2^\pi$ . Observe that this line is *not* crossed by any unbending line (See text for details).

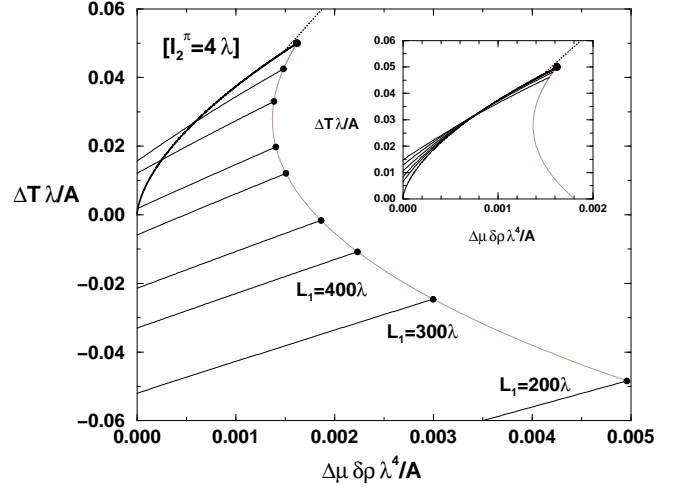


FIG. 7. As Fig. 6, with  $\ell_2^\pi = 4\lambda$  and  $L_1 = 2, 3, 4, 5, 7.5, 10, 20$  and  $50 (\times 10^2\lambda)$ . Inset: Merging of the unbending line with the pre-wetting line for large stripe widths,  $L_1 = 1, 2, 4, 8$  and  $16 (\times 10^4\lambda)$ .

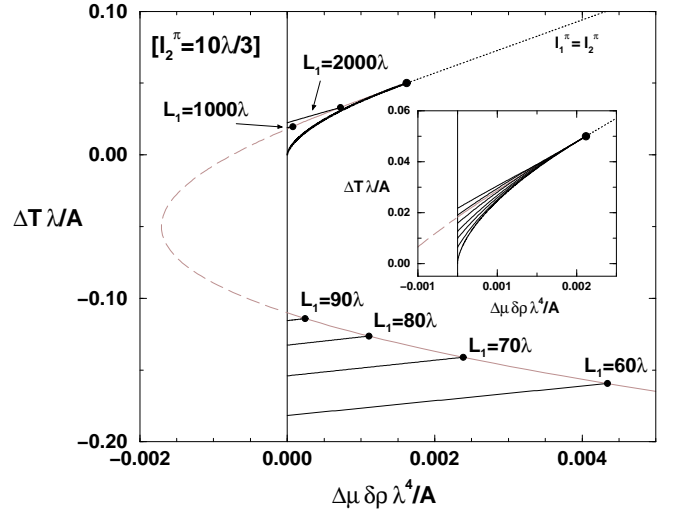


FIG. 8. As Fig. 6, with  $\ell_2^\pi = 10\lambda/3$  and different values of  $L_1$ . The grey broken line is the loci of the unbending critical points that have been pre-empted by the bulk liquid-vapour phase transition. Inset: Merging of the unbending line with the pre-wetting line for large stripe widths,  $L_1 = 4, 8, 16, 32$  and  $64 (\times 10^3\lambda)$ .

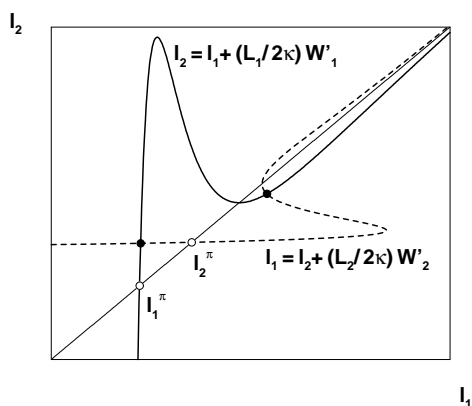


FIG. 9. Sketch of the graphical construction used to solve equations (30). In the figure, both potentials  $W_1$  and  $W_2$  represent first order wetting transitions. The solutions correspond to the intersection of the curves  $l_2 = l_1 + \frac{L_1}{2\kappa} W'_1(l_1)$  and  $l_1 = l_2 + \frac{L_2}{2\kappa} W'_2(l_2)$  (black circles). If there are more than one, as in the figure, the stable one will have the lower free energy, Eq. (5). The thickness of the adsorbed layers on the pure substrates  $l_1^\pi$  and  $l_2^\pi$  correspond to a crossing of the curves with the line  $l_1 = l_2$  (white circles).

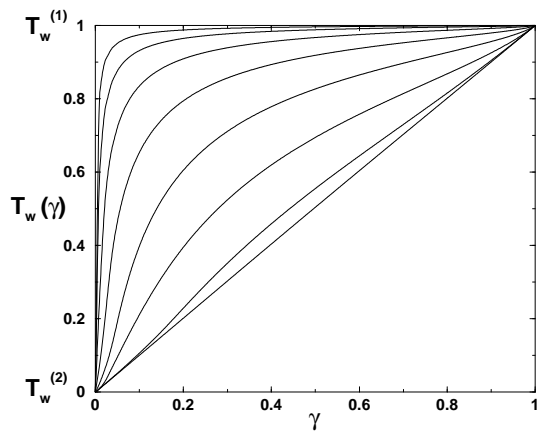


FIG. 10. Wetting temperature (measured with respect to  $T_w^{(2)}$ ) of a periodic heterogeneous substrate calculated with the minimal model, Eq. (5) and the effective potentials (39) and (40). The wetting temperature (in units of  $A_1/\lambda$ ) is represented as a function of the fractional area of the first material,  $\gamma$ , for different values of the period  $L/\lambda = 1, 10, 10^2, 10^3, 10^4, 10^5, 10^6$  and  $10^7$  (from below). We use the following parameters:  $T_w^{(1)} - T_w^{(2)} = A_1/\lambda$ ,  $B_1 = 2B_2 = A_1\lambda$ ,  $A_1 = A_2$  and  $\alpha = 2$ .

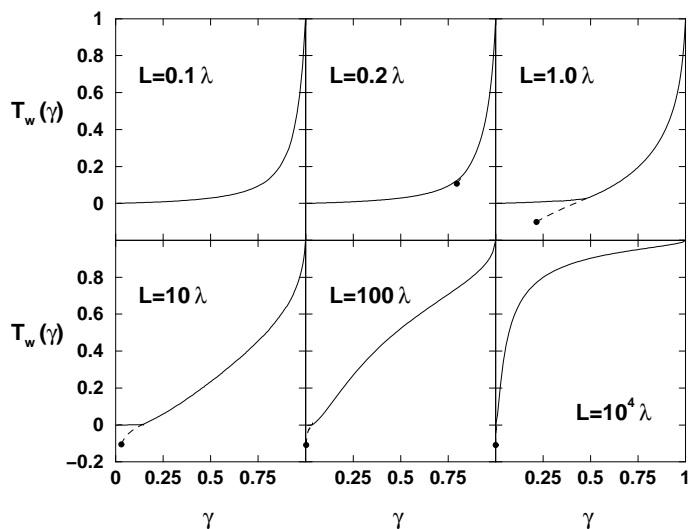


FIG. 11. As Fig. 10, for  $T_w^{(1)} - T_w^{(2)} = A_1/\lambda$ ,  $B_2 = 4B_1 = 2A_1\lambda$ ,  $A_2 = 0.05A_1$  and  $\alpha = 20$ . The broken line represents an unbending coexistence line appearing for  $L \approx 0.2\lambda$  (see text for details).

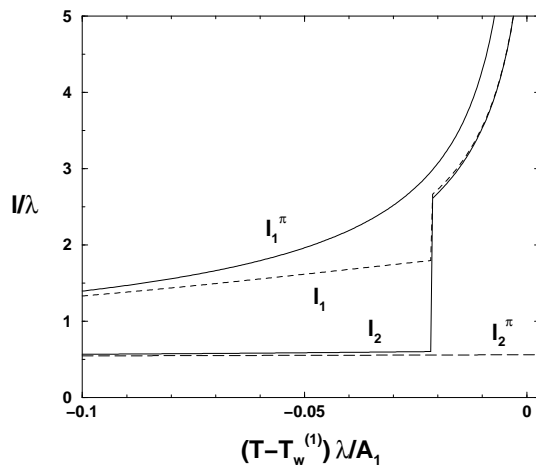


FIG. 12. Adsorption on the periodic system whose wetting temperature is plotted in Fig. 11 for  $L = 10\lambda$  and  $\gamma = 0.1$ . The curves  $l_1$  and  $l_2$  represent the adsorption on the substrates 1 and 2 (respectively). A (first-order) unbending transition takes place for  $(T - T_w^{(1)})\lambda/A_1 \approx -0.02$ . For the sake of comparison, the adsorption on the pure substrates 1 and 2 is also shown ( $l_1^\pi$  and  $l_2^\pi$ ).

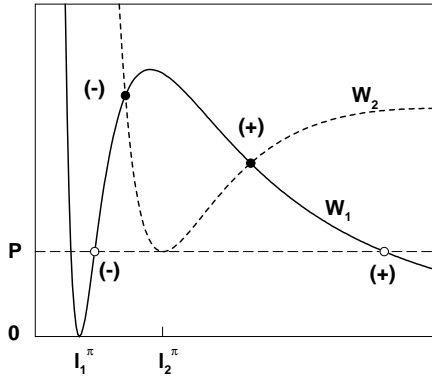


FIG. 13. Geometrical construction to solve Eq. (A3) for arbitrary effective potentials  $W_1$  and  $W_2$  at  $T = T_w^{(1)}$ .  $W_1$  shows an activation barrier, necessary to model a first-order wetting transition. There are two possible solutions for both  $\ell_0$  (empty circles) and  $\ell_L$  (black circles). These correspond to bound (-) and near-unbound (+) interfacial configurations.